



Solar-pumped dual-rod Ce:Nd:YAG laser with 58 W continuous-wave output power and 5.1° tracking error compensation width

JOANA ALMEIDA,¹ DAWEI LIANG,^{1,*}  MIGUEL CATELA,¹
HUGO COSTA,¹ DÁRIO GARCIA,¹ BRUNO D. TIBÚRCIO,¹
EMMANUEL GUILLOT,²  AND CLÁUDIA R. VISTAS¹

¹*Centro de Física e Investigação Tecnológica (CEFITEC), Departamento de Física, Faculdade de Ciências e Tecnologia, Universidade NOVA de Lisboa, 2829-516 Caparica, Portugal*

²*Procédés, Matériaux et Énergie Solaire - Centre National de la Recherche Scientifique (PROMES-CNRS), 7 rue du Four Solaire, 66120 Font-Romeu-Odeillo-Via, France*

*dl@fct.unl.pt

Abstract: The pursuit of high-power solar laser systems with high efficiency and capacity for large tracking error compensation is determinant for the applicability of this renewable technology. A side-pumped dual-rod Ce:Nd:YAG solar laser was developed and tested at the focus of a 2 m diameter parabolic concentrator. Maximum continuous-wave total solar laser power of 58 W was measured. To the best of our knowledge, this is the highest laser power from a Ce:NdYAG solar laser. Moreover, wide tracking error compensation width of 5.1° in the azimuthal direction was reached, being 4.25 times higher than the previous measurement without solar tracking assistance.

© 2023 Optica Publishing Group under the terms of the [Optica Open Access Publishing Agreement](#)

1. Introduction

Solar-pumped laser uses solar energy for pumping an active medium, directly converting incoherent solar radiation into coherent laser radiation. It can be considered as one of the most promising technologies in renewable energy and laser technology research [1], being especially suited for space-based applications, such as free space optical communications, power transmission and laser propulsion [2–4]. Therefore, solar-pumped laser may be used as a noncontact method to transmit the converted solar energy across large distances, from space to either deep space or earth, which may pave the way for the future development of sustainable industrialization in space. Specific applications of solar-pumped lasers may also include the removal of orbital debris and asteroid deflection [5,6]. This renewable technology has also attracted attention owing to its potential applicability in terrestrial applications, such as fossil-fuel free energy cycles [7,8]. Its application can also involve the illumination of photovoltaic cells for high solar-to-electrical conversion efficiency, which can be used to feed electric-drive vehicles [9].

The first laser directly pumped by solar radiation was reported by Kiss et al. in 1963, with calcium fluoride crystal doped with divalent dysprosium ($\text{Dy}^{2+}:\text{CaF}_2$) as the active medium, achieving continuous-wave (cw) solar laser action at 2.36 μm [10]. Since then, several active media have been investigated as candidates for solar-powered lasers. Still, substantial progress in this research had occurred with bulk solid-state optical gain media, namely with the yttrium aluminum garnet ($\text{Y}_3\text{Al}_5\text{O}_{12}$) doped with the rare earth ion neodymium (Nd^{3+}) emitting at 1064 nm [11–19] owing to the favorable combination of the spectroscopic properties of the Nd^{3+} active ion with the mechanical and optical properties of the YAG host material [20].

Although Nd:YAG is the most common laser medium employed in solar-pumped lasers [11–19], Nd^{3+} ions are not ideal dopants due to the low spectral overlap of 14–16% between the

Nd^{3+} absorption spectrum and the blackbody-like solar emission spectrum [13,21], imposing limits to the efficiency of solar lasers. Attempts have been made to improve the solar laser efficiency by co-doping the Nd:YAG medium with sensitizers, such as chromium (Cr^{3+}) [22,23] and cerium (Ce^{3+}) ions [24–30], due to their broader absorption band to overlap with the solar emission spectrum [31,32]. Records in collection efficiency (laser output power per each square meter of primary concentrator area), slope efficiency (slope of the laser output power variation with the incoming solar power) and solar-to-laser conversion efficiency (the ratio between solar laser output power and corresponding incoming solar power) of $32.5 \text{ W}\cdot\text{m}^{-2}$, 6.7% and 3.74%, respectively, were attained in 2018 by end-side-pumping a Cr:Nd:YAG single-rod through a primary parabolic concentrator [23]. Even so, breakthroughs on solar laser efficiency were attained more recently with the adoption of Ce:Nd:YAG as the laser medium [25–30]. The Ce:Nd:YAG has two strong and broad absorption bands in the ultraviolet and visible region, which overlaps well with the solar spectrum region of higher intensity, and possesses other absorption bands in the red and near infrared region, which are characteristic of the Nd^{3+} ions. Besides that, efficient energy transfer from Ce^{3+} to Nd^{3+} ions in the Ce:Nd:YAG material occurs via both radiative and non-radiative mechanisms [33,34]. In 2022, Garcia et al. reported the most efficient single-rod solar laser with $38.2 \text{ W}\cdot\text{m}^{-2}$ collection efficiency, 6.8% slope efficiency and 4.5% solar-to-laser conversion efficiency, by end-side-pumping a thin Ce:Nd:YAG rod through a heliostat-parabolic mirror system with an effective collection area of only 0.293 m^2 [26]. $38.8 \text{ W}\cdot\text{m}^{-2}$ single-rod Ce:Nd:YAG solar laser was also achieved in that year by Cai et al., who used a 0.69 m^2 Fresnel lens solar energy collection and concentration system [27].

In end-side-pumping configurations, most of the concentrated solar radiation is directly focused onto the end face of the laser rod, i.e., parallel to the laser beam. Therefore, the optical path of solar rays within the laser medium is much longer than that of side-pumping schemes, enabling higher pumping efficiency. Nevertheless, this pumping configuration can lead to severe thermal loading issues in single solid-state laser media of cylindrical geometry, especially at higher solar power levels, due to the non-homogenous pumping light distribution along the laser rod's length. This can preclude solar laser systems to scale to high powers, especially those with Ce:Nd:YAG as active medium whose thermal effects are more pronounced with solar pumping compared to Nd:YAG material, which may lead to laser rod damage [24]. To try to solve this issue, the potential of multirod solar laser systems for laser power scaling, based on the simultaneous pumping of several laser media, has been experimentally tested by Liang et al. [19,28]. In these systems, each rod absorbs only a portion of the concentrated solar radiation incident on the pumping cavity, reducing significantly the thermal induced effects. Currently, the records in collection, slope and solar-to-laser conversion efficiencies of $41.3 \text{ W}\cdot\text{m}^{-2}$, 7.64%, and 4.64%, respectively, were attained through the simultaneous pumping of three Ce:Nd:YAG laser rods by a heliostat-parabolic mirror system [28]. Still, the maximum input solar powers used for evaluating the Ce:Nd:YAG solar laser performance did not exceed 470 W.

Side-pumping configuration is suitable for laser power scaling as it allows an even pump light distribution along the laser rod axis, minimizing the thermal loading problems. Therefore, efforts were also made to improve the Ce:Nd:YAG solar laser efficiency at higher input power levels with side-pumping configurations [25,29,30]. For 1125 W incoming solar power at the medium size solar furnace of Procédés, Matériaux et Énergie Solaire - Centre National de la Recherche Scientifique (PROMES-CNRS), the maximum cw solar laser power of 19.6 W was emitted from a 4 mm diameter, 35 mm length Ce(0.1 at.%):Nd(1.1 at.%):YAG laser rod, leading to $18 \text{ W}\cdot\text{m}^{-2}$, 3.03% and 1.74% collection, slope and conversion efficiencies, respectively [29]. To preserve the concentrated solar radiation profile for efficient side-pumping of the laser rod, an aspherical lens was used as a secondary concentrator. However, this has resulted in an uneven light distribution along the laser rod, which led to its fracture when adding more incoming solar power. To reduce the accumulated heat within the laser medium, a solar laser head with a rectangular light guide

as secondary concentrator was employed to uniformly side-pump the same Ce:Nd:YAG rod under similar pumping conditions [29,30]. Despite the decrease in the solar laser efficiency with increasing collection area, the side-pumping configuration with light-guide allowed the Ce:Nd:YAG laser rod to withstand an elevated incoming solar power level of 2600 W, producing 40 W cw solar laser power with the maximum effective collection area of the parabolic mirror [30]. This was the highest reported cw solar laser power emitted from a Ce:Nd:YAG solar laser medium.

In order to achieve the aforementioned breakthroughs, primary concentrators with high concentration ratios, such as parabolic mirrors, were required to harvest sunlight for efficient pumping of bulk solid-state laser media [23,25,26,28–30]. In turn, this high-concentration optics needs mechatronic devices for precise tracking of the apparent movement of the sun along the day in order to keep the focal spot aligned with the solar laser head, which may limit the practicability of solar-pumped lasers. Besides, a solar tracking system with an error below 0.2° can cost about 10 times more than a similar system with twice the solar tracking error [35], increasing the costs of solar laser systems. To reduce the need for expensive sun-tracking systems, several multirod solar laser systems with either end-side-pumping [36–38] or side-pumping configurations [39,40] have been numerically investigated by our research team with the aim of achieving high tracking error compensation capacity. In 2022, Tibúrcio et al. reported the first experimental results in solar laser tracking error compensation capacity by using a side-pumped dual-rod solar laser head at the focus of a heliostat-parabolic mirror system [41]. Maximum total laser power of 14.8 W was recorded from two Nd:YAG laser rods. The solar laser power variation with no sun tracking was then registered for one minute, by stopping the operation of the heliostat during that time. Maximum tracking error compensation width of 1.4° at 10% laser power loss ($TEW_{10\%}$) was calculated. This study demonstrated the significance of pumping more than one laser rod simultaneously within a single cavity in providing stable solar laser beam emission with enhanced thermal performance, while helping to reduce the need for expensive solar trackers [41]. Still, the potential of this system to scale to higher laser power and efficiency was limited by the use of the Nd:YAG active media. Besides, further optimization of the pumping cavity could be done to augment the solar tracking error width, especially in the azimuthal direction, which mostly influences the solar laser performance around the solar noon [37,41,42].

Due to the aforementioned reasons, a dual-rod side-pumping laser head was developed for the simultaneous emission of two high-power Ce:Nd:YAG solar laser beams with enhanced efficiency and tracking error compensation capacity. The present solar laser head, composed of a $22\text{ mm} \times 68\text{ mm}$ double-stage dry pump cavity, a long fused silica flow tube and the two thin and long Ce(0.1 at. %):Nd(1.1 at. %):YAG solar laser rods with 3 mm diameter and 80 mm length, was mounted and tested at the focus of the 2 m diameter parabolic mirror of PROMES-CNRS. The wide pump cavity, consisting of a rectangular hollow pipe and a two-dimensional concentrator of biconical shape, along with the long fused silica tube, played a crucial role in guaranteeing both an efficient focusing and efficient redistribution of the highly concentrated solar radiation along the laser rods, while avoiding the transmission losses associated with the use of fused silica light guides [30,41]. Maximum cw total laser power of 58 W was registered with the full effective collection area of the parabolic mirror of 2.3 m^2 . This was the highest reported cw laser power value from a Ce:Nd:YAG solar laser, being 1.45 times higher than that from the previous Ce:Nd:YAG solar laser head with rectangular light guide [30]. Collection, slope and solar-to-laser conversion efficiencies of $25.3\text{ W}\cdot\text{m}^{-2}$, 3.75% and 2.62% were attained, respectively, resulting in enhancements of 1.57, 1.54 and 1.7 times over the previous results from the 40 W Ce:Nd:YAG solar laser side-pumped at PROMES-CNRS [30]. In addition, the longest solar laser operation with no solar tracking was also registered during 280 seconds, with total laser power loss of less than 10%. Consequently, highly stable solar laser emission with record tracking error compensation width of 5.1° was attained.

2. Materials and methods

2.1. Solar energy collection and concentration system

The present dual-rod Ce:Nd:YAG solar laser was tested in the medium size solar facility of PROMES-CNRS. As shown in Figs. 1(a) and (b), this solar facility is constituted by a two-axis heliostat and a stationary parabolic concentrator. The heliostat has 36 flat mirror segments, each with $0.5 \text{ m} \times 0.5 \text{ m}$ dimensions, which tracks and redirects the solar radiation to the parabolic mirror with 2.0 m diameter, 0.85 m focal distance and 60° rim angle [29,30].

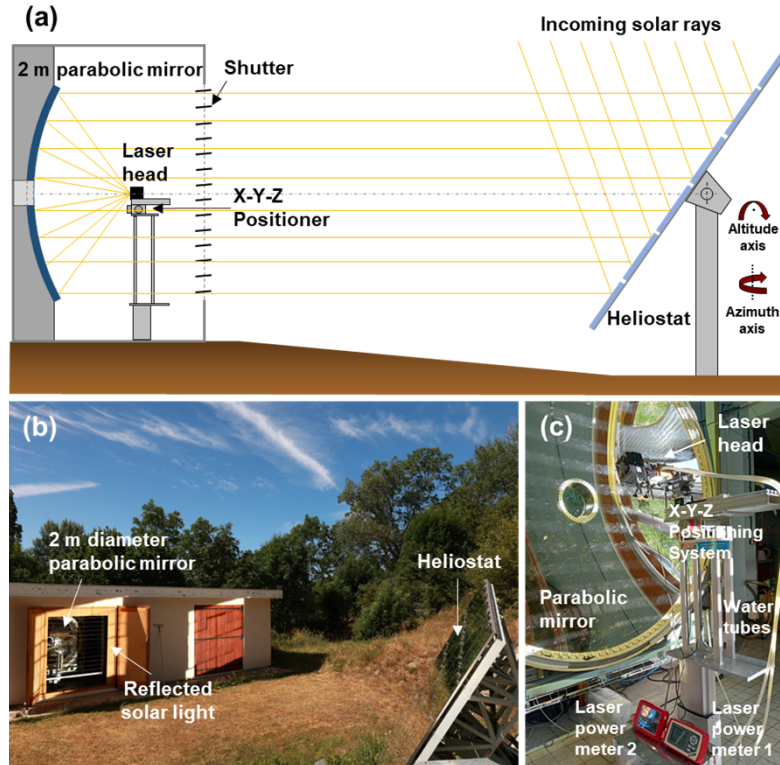


Fig. 1. (a) Schematic design of the solar energy collection and concentration system for the dual-rod Ce:Nd:YAG laser. Photographs of the (b) PROMES-CNRS medium size solar facility and (c) the dual-rod Ce:Nd:YAG solar laser head mounted at the focus of the 2 m diameter parabolic mirror.

Both heliostat and parabolic mirrors are back silvered, each with less than 80% reflectivity because of the iron contents in the glass substrate and degradation owing to many years of usage. Consequently, about 59% of the incoming solar rays reach the focus of the parabolic mirror [29,30].

The dual-rod Ce:Nd:YAG solar laser head, along with the resonant cavity from each rod, was fixed on a mechanical support with automatic X-Y-Z axis calibration at the focal zone of the parabolic concentrator, as shown in Figs. 1(a) and (c). The laser output powers from each rod were detected by two power meters.

2.2. Side-pumped dual-rod Ce:Nd:YAG solar laser head

The design of the dual-rod Ce:Nd:YAG solar laser head is illustrated in Fig. 2. It consisted of the double-stage dry pump cavity, formed by a rectangular hollow pipe and a two-dimensional

concentrator of biconical shape, and the fused silica flow tube, within which the two thin Ce:Nd:YAG rods with 3 mm diameter and 80 mm length were fixed and cooled by water.

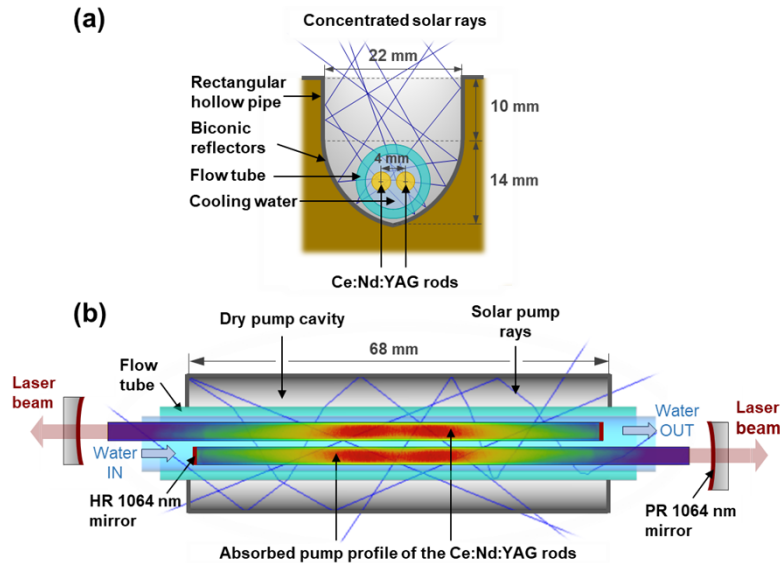


Fig. 2. (a) Front-view and (b) top-view of the dual-rod/dual-beam Ce:Nd:YAG solar laser head design. The laser resonant cavities and absorbed pump profiles of the two laser rods are also represented in (b).

As shown in Fig. 2(a) and 2(b), the hollow pipe with 22 mm \times 68 mm input aperture collected and redistributed the concentrated solar radiation from the focus of the parabolic mirror to the 22 mm \times 68 mm entrance aperture of the secondary concentrator of 14 mm depth, composed of two symmetric biconic reflectors with 14.5 mm radius of curvature and conic constant = 0, which allowed efficient focusing of the concentrated solar rays with different incident angles along the two Ce:Nd:YAG laser rods, with their central axes spaced 4 mm apart. The 77 mm length fused silica flow tube of 99.995% optical purity (supplied by CBMA Quzhou Kinglass Quartz Co. Ltd.), with external/internal diameters of 12 mm / 9 mm, had a crucial role in the pumping efficiency. Due to the difference of refraction index n between the air ($n_{air} = 1$) and the water coolant ($n_{water} = 1.33$), the flow tube acted as a lens, helping to refocus both the direct concentrated solar rays and the reflected solar rays from the dry pumping cavity to the laser rods. Cooling water provided by the laboratory plumbing system, with 4.5 bar at room temperature (15–20 °C), was used for removing the heat generated on the laser rods inside the flow tube.

The internal walls of the dry pump cavity were covered with silver-coated aluminum foils of 94% reflectivity for efficient absorption of the solar pumping wavelengths by the Ce:Nd:YAG active media [28–30]. These foils were also used to cover the top of the brass mechanical components of the solar laser head, as shown in Fig. 3, in order to protect them from heating.

The mechanical fixation of the laser rods was designed to allow the emission of the two solar laser beams in opposite directions, as observed in both Figs. 2(b) and 3(a), suitable for future utilization in different laser applications simultaneously. The laser resonant cavity of each laser rod was hence formed by the high reflection (HR) coatings at the laser emission wavelength (>99.5% @ 1064 nm) deposited on one end-face of the rods and a partial reflection (PR) coated mirror (~94% @ 1064 nm) aligned with the optical axis of the active medium, on the opposite side of the HR (Fig. 2(b)). The 3 mm diameter, 80 mm length Ce(0.1 at.%):Nd(1.1 at.%):YAG rods were manufactured by Chengdu Dongjun Laser Co., Ltd. The end faces of the laser rods

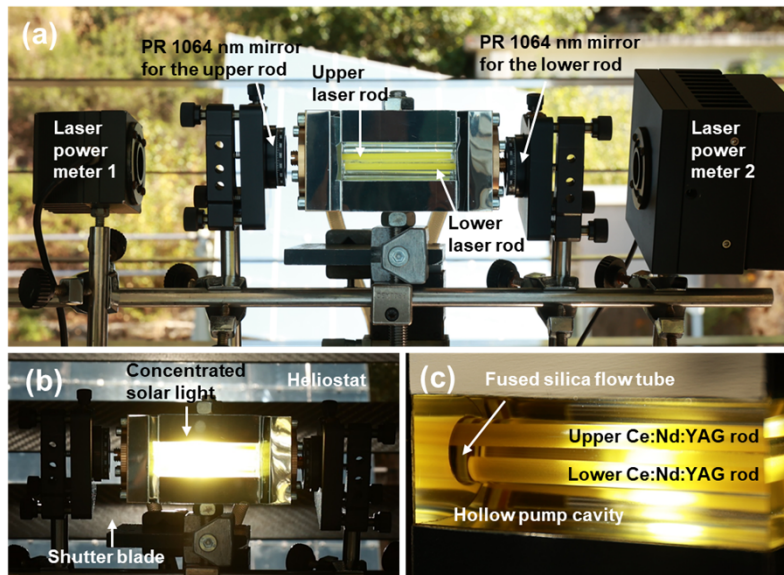


Fig. 3. Photograph of the dual-rod Ce:Nd:YAG solar laser head and laser resonators at the focus of the parabolic mirror (a) without and (b) with attenuated incident concentrated solar light. (c) Detailed view of the two Ce:Nd:YAG rods inside the flow tube within the dry pump cavity.

closer to the PR mirrors were covered with anti-reflective (AR) coating for 1064 nm ($<0.2\%$ @ 1064 nm). The PR laser mirrors were supplied by ESKMA Optics.

The present prototype was designed and developed in Lisbon from January to July 2023. It was then tested at the 2 m diameter parabolic mirror of the PROMES-CNRS from July 24 to July 28, 2023.

3. Experimental results and discussion

The dual-rod Ce:Nd:YAG solar laser experiments consisted in the evaluation of its capacity to 1) scale to higher power laser levels and 2) compensate for large solar tracking errors. In both experiments, the solar laser operated in multimode regime for maximum extraction of cw laser output power. As shown in Fig. 3(a), the PR mirrors were optically aligned as close as possible to their respective laser rods (approximately 30 mm away from the AR end faces), each forming a short laser resonator of similar total length of about 110 mm. PR mirrors with 94% reflectivity and -1 m radius of curvature were adopted for both laser resonators for efficient extraction of multimode laser power [43,44]. Laser output powers were detected by S310C and S322C thermal power sensor heads and displayed by PM100D and PM200 digital power meter consoles, respectively, from Thorlabs. The solar irradiances were also measured during the experiments with a Kipp & Zonen CH1 pyrhelimeter on a Kipp & Zonen 2AP solar tracker.

3.1. Dual-rod Ce:Nd:YAG solar laser output measurements as a function of incoming solar power and collection area

To study the scalability of the present Ce:Nd:YAG solar laser system to higher power levels, its performance was tested as a function of the incoming solar power at five different diameters (D) of the parabolic mirror, by masking its external annular area correspondingly, starting from a relatively small diameter ($D = 1.33$ m) to its maximum diameter ($D = 2.00$ m), as indicated

in Fig. 4. The performances of the previous single-rod side-pumped Ce:Nd:YAG solar laser systems tested in the same solar facility are also given in Fig. 4 for comparison [29,30].

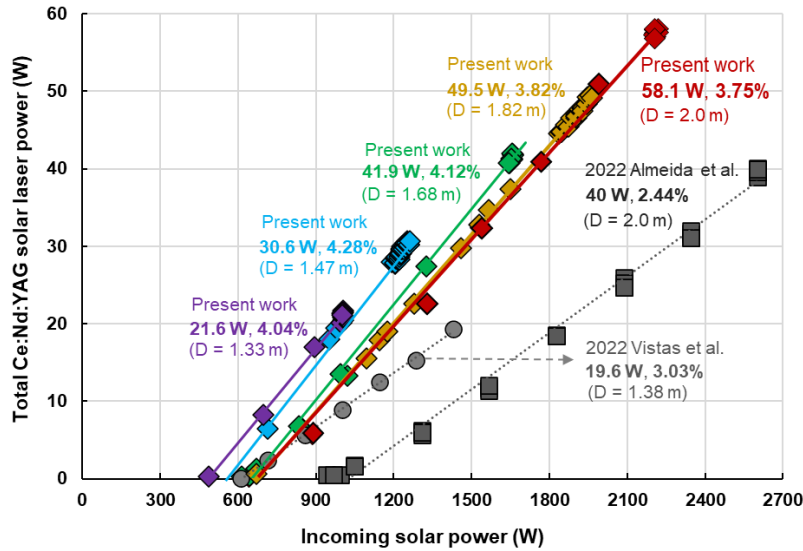


Fig. 4. Total solar laser power from the two Ce:Nd:YAG rods as a function of the incoming solar power and parabolic mirror diameter (D) at PROMES-CNRS. Previous experimental results from the single-rod Ce:Nd:YAG solar lasers pumped by the same solar facility, with aspherical lens [29] and light guide [30] as secondary concentrators, are also given.

During the experiments of the dual-rod Ce:Nd:YAG solar laser, the solar irradiances varied from 900 to 1005 $\text{W}\cdot\text{m}^{-2}$. The incoming solar power was regulated by a shutter with motorized blades (Fig. 3(b)). All the shadow effects in the parabolic mirror caused by the space between the flat mirrors of the heliostat, the shutter blades, the laser head, and respective mechanical supports, have been accounted for calculating the effective collection area and, consequently, the effective incoming solar power.

As shown in Fig. 4, the variation of the parabolic mirror diameter influenced the performance of the dual-rod Ce:Nd:YAG laser. Solar laser emission started earlier with smaller collection diameter of $D = 1.33$ m, reaching maximum total laser power of 21.6 W from the two rods at an incoming solar power of 1005 W and a slope efficiency of 4.04%. Still, the best slope efficiency of 4.28% was reached at $D = 1.47$ m. In this case, maximum total laser power of 30.6 W was achieved. With the increase of the parabolic mirror diameter, the slope efficiency decreased. A similar tendency has already been observed in previous solar laser experiments with Nd:YAG [45] and Ce:Nd:YAG laser media [28,30], using a parabolic mirror as primary concentrator. Therefore, we can assume that there is an optimal collection area, as well as an optimal angle of light incidence, where the solar laser system can provide the best performance. Nevertheless, despite the decrease in slope efficiency, the dual-rod Ce:Nd:YAG solar laser power has progressively increased to maximum values of 41.9 W, 49.5 W and finally 58.1 W at $D = 1.68$ m, $D = 1.82$ m and $D = 2.00$ m, respectively, with no damage to the laser rods. These were, to the best of our knowledge, the highest reported cw Ce:Nd:YAG solar laser powers. This means that the previous record in Ce:Nd:YAG laser power of 40 W, attained at the PROMES-CNRS solar facility with $D = 2.00$ m and incoming power of 2600 W [30], was surpassed by the present scheme at a much lower incoming power of 1656 W and collection diameter of 1.68 m. Slope efficiency of 4.12% was found in this case, being 1.69 times better than that from the previous 40 W cw Ce:Nd:YAG solar laser [30].

The maximum cw output power of 58.1 W resulted in an enhancement of 1.45 times in relation to the previous solar laser power record [30] and in a three-fold increase in relation to that from the previous single-rod Ce:Nd:YAG solar laser side-pumped by an aspherical lens secondary concentrator at the same solar facility [29]. Although the slope efficiency had decreased to 3.75% in this case, it was still 1.54 and 1.24 times better than the previous side-pumped Ce:Nd:YAG solar lasers with light-guide [30] and aspherical lens secondary concentrators [29], respectively, tested in PROMES-CNRS.

Table 1 resumes the dual-rod Ce:Nd:YAG solar laser performance at the highest solar laser power in terms of threshold solar power, maximum solar laser and incoming powers, slope, solar-to-laser conversion and collection efficiencies. The performances of the previous side-pumped Ce:Nd:YAG solar lasers tested at PROMES-CNRS are indicated for comparison. The corresponding M^2 beam quality factors are also given.

As can be seen in Table 1, in addition to superior power and slope efficiency, the dual-rod Ce:Nd:YAG solar laser was also superior in solar-to-laser conversion and collection efficiencies. 2.62% solar-to-laser conversion efficiency was reported, revealing an improvement of 1.5 and 1.7 times over that from the single-rod Ce:Nd:YAG solar lasers side-pumped by the aspheric lens [29] and light-guide [30], respectively. 25.3 W.m⁻² collection efficiency was also reached by the present prototype, being 1.41 and 1.57 times higher than that from the previous schemes tested at PROMES-CNRS [29,30]. This value also surpassed by 1.07 times the previous record in side-pumped solar laser collection efficiency with Ce:Nd:YAG medium [25]. Compared to the previous single-rod Ce:Nd:YAG solar laser with 40 W laser output power [30], the dual-rod Ce:Nd:YAG solar laser also enabled a 1.47 times reduction in threshold solar power and better M^2 beam quality factors. The Ce:Nd:YAG solar laser pumped by aspheric lens presented better results in these parameters [29]. However, it should be noted that its performance was evaluated utilizing a 1.38 m collection diameter of the parabolic mirror and maximum incoming power of 1125 W. Above that, the Ce:Nd:YAG laser rod was damaged due to the thermal load caused by the inhomogeneous pumping, as illustrated in Table 1. This reveals the importance of having an even solar pumping distribution across the laser rods for solar laser power scaling. The efficient redistribution of the pump light along the two thin and long Ce:Nd:YAG laser rods in the present scheme was crucial to alleviate the thermal lensing effects in the active media, helping to scale not only the laser power but also the efficiency of solar laser with side-pumping configuration. It also helped to improve the solar laser beam quality at high input power levels.

Figure 5 shows the near circular and homogeneous multimode laser beam profile from one of the two Ce:Nd:YAG rods of the present prototype, registered with a CINOGY UV-NIR beam profiler - CinCam CMOS positioned 0.2 m away from the PR mirror.

3.2. Dual-rod Ce:Nd:YAG solar laser tracking error compensation capacity measurements

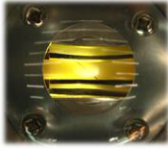
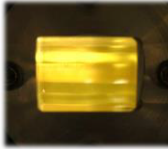

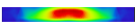
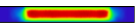
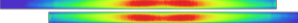
The sun appears to move across the sky during the day due to the rotational motion of the earth. The sun's path across the sky also varies seasonally and with geographical location. The earth's axial tilt of approximately 23.5° and its elliptical orbit around the sun ensures that observers at different locations will see the sun motion differently throughout the year [46].

This apparent motion can be described by means of two astronomical angles – the solar azimuth and the solar altitude [42].

The solar azimuth angle (α) is the angle of sun's rays in the horizontal plane and it is dependent on the hour (ω), declination (δ), and altitude (h) angles by [47]:

$$\sin(\alpha) = \frac{\sin(\omega) \cos(\delta)}{\cos(h)} \quad (1)$$

Table 1. Resume of the Ce:Nd:YAG solar laser performances from the present and the previous side-pumping prototypes tested at PROMES-CNRS solar facility

Parameters	2022 Vistas et al. [29]	2022 Almeida et al. [30]	Present Ce:Nd:YAG solar laser	Improved over [29] / [30] [times]
Solar laser head (Photo / Characteristics)	 Aspheric Lens + 2V-shaped pump cavity	 Light-guide + V-shaped pump cavity	 Dry pump cavity (Hollow pipe + Biconic concentrator)	n/a ^a
Laser rod dimensions (Qty.)	∅4 mm × 35 mm (1)	∅4 mm × 35 mm (1)	∅3 mm × 80 mm (2)	n/a
Absorbed pump profile ^b				n/a
Collection diameter	1.38 m	2.00 m	2.00 m	n/a
Threshold solar power	480 W	943 W	641 W	--- / 1.47 times reduction
Maximum solar laser power	19.6 W	40.0 W	58.1 W	2.96 / 1.45
Maximum incoming solar power	1125 W	2600 W	2218 W	n/a
Slope efficiency	3.03%	2.44%	3.75%	1.24 / 1.54
Solar-to-laser conversion efficiency	1.74%	1.54%	2.62%	1.5 / 1.7
Collection efficiency	18.0 W.m ⁻²	16.1 W.m ⁻²	25.3 W.m ⁻²	1.41 / 1.57
M ² _x , M ² _y factors	30, 30	52, 54	34.4, 36.6 (for each rod)	--- / 1.49 times reduction

^aNot applicable; ^bSimulated in Zemax® optical software

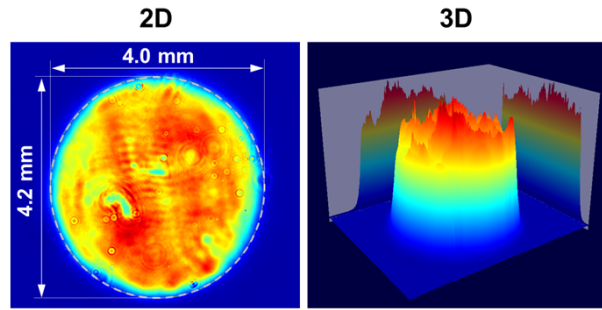


Fig. 5. Measured 2D and 3D laser beam profiles from one of the rods of the dual-rod Ce:Nd:YAG solar laser head, 0.2 m away from the output mirror.

The solar altitude (or elevation) angle (h) is defined as the angle between the sun ray's projection on the earth and its horizon plane. It is related to both the hour angle (ω) and the declination angle (δ) by the following equation [47]:

$$\sin(h) = \cos(\omega) \cos(\varphi) \cos(\delta) + \sin(\varphi) \sin(\delta) \quad (2)$$

where φ is the local latitude.

The solar altitude angle (h) at the time of sunrise and sunset is 0° and has its maximum value at solar noon time in all seasons [42].

The hour angle (ω) is used to describe the earth's rotation about its polar axis, corresponding to the angle between the meridian passing through the sun and the meridian of the observer on earth. It can be given by [47]:

$$\omega = \pm 0.25^\circ \times t \quad (3)$$

where t is the time in minutes from local solar noon. The hour angle at local solar noon is zero. Therefore, the minus sign is applied to the hour angles before local noon (morning) and the plus sign is applied to the hour angles after the local noon (afternoon).

The solar declination (δ) is the angle between the line joining the centers of the sun and the earth and its projection on the equatorial plane. It can be approximately calculated for any day of the year (d) by the following equation [47]:

$$\delta = 23.45^\circ \sin \left[\frac{360}{365} (284 + d) \right] \quad (4)$$

These equations are fundamental for calculating the solar laser tracking error compensation capacity [37,42]. The conventional heliostat configuration, as in the case of the PROMES-CNRS heliostat, is based on the variation of two axes simultaneously – the azimuth axis and the altitude axis, related to the azimuth and altitude solar angles. The azimuth axis is vertical relative to the heliostat base, tracking the angle bisector between the sun and the receiver in the east-west direction. The altitude axis is normal to the azimuth axis, tracking the sun in north-south direction [48]. Therefore, the variations in azimuth and altitude angles can be assumed as azimuth and altitude solar tracking errors, respectively.

For accurate evaluation of the tracking error compensation capacity of the present solar laser, the measurement was done during a clear sky period to guarantee nearly constant solar irradiance values during the trial. For such, it was also essential to realize this evaluation around the local solar noon in PROMES-CNRS. The parabolic mirror collection diameter of 1.47 m was used in this experiment.

Analogously to the previous tracking error compensation measurements by Tibúrcio et al. [41], the present experiment was also initiated with the solar facility (heliostat + parabolic mirror)

precisely aligned with the sun to ensure optimal solar pumping. Once the automatic sun tracking was activated in the heliostat control panel, the shutter blades were open at 60% of their full opening capacity for precise X-Y-Z position alignment of the center of the pumping cavity entrance aperture with the focal spot, while avoiding overheating of the laser head. The accuracy of this alignment was also confirmed by the similarity of the laser output powers emitted by each laser rod, as demonstrated in Fig. 6 at the initial time of the measurement ($t = 0$ s). The automatic sun tracking was then stopped in the heliostat panel control and the individual laser output powers from each rod were registered during 280 s.

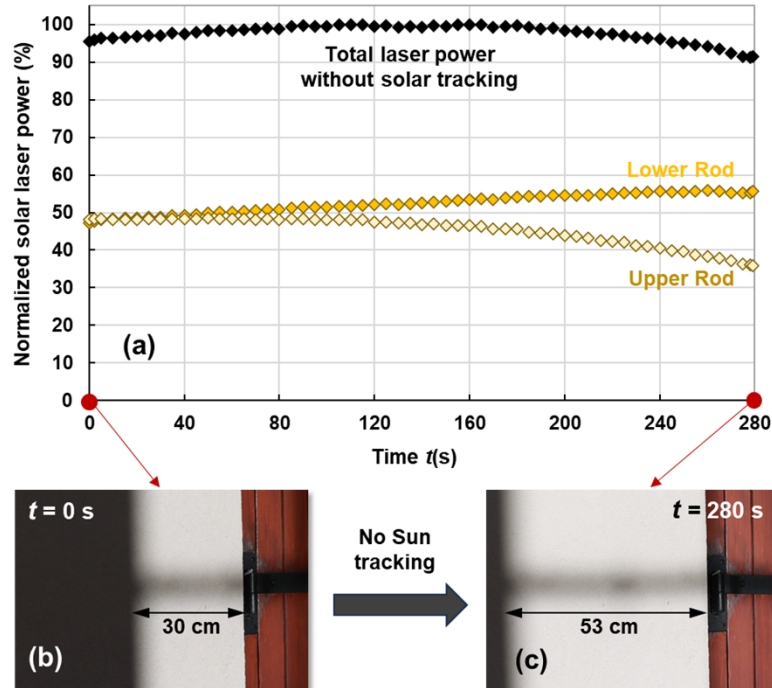


Fig. 6. (a) Normalized solar laser output power of the dual-rod Ce:Nd:YAG solar laser without solar tracking during 280 s, as well as the corresponding normalized laser power from each rod. The photographs show the reflected solar light from the heliostat to the laboratory entrance (in front of the shutter): (b) with optimal alignment ($t = 0$ s) and (c) after 280 s with no solar tracking.

Figure 6 shows the normalized solar laser output powers from each laser rod, as well as the total solar laser output power, during the 280 s with no sun tracking. Since the sun apparently kept changing its position along the sky, the interruption of the solar tracking system during the 280 s led to a displacement of about 23 cm of the reflected solar light from the heliostat at the laboratory entrance (in front of the shutter), as demonstrated by the photographs in Fig. 6. This consequently affected the apparent movement of the focal spot along the pumping cavity, leading to the variation of the solar laser output power from each laser rod. Still, it is worth noting that this variation only started to be more noticeable after 80 s (1 minutes 20 seconds) of no sun tracking. Besides, while the laser output power from the upper rod started to decrease from then on, the laser output power from the lower rod was slightly increasing, leading to stable total laser power emission during 280 s. In that instant, the normalized total laser power was still above 90% of its initial value. This was, as far as we are aware, the longest period a solar laser has operated with no solar tracking and with high stability. During this experiment, the solar irradiances varied only slightly, from 992 to 995 $\text{W}\cdot\text{m}^{-2}$, also contributing to highly stable solar laser emission.

The abovementioned equations (1–4) were then used to calculate the apparent variation of the sun's position in both altitude and azimuthal directions (in degrees) during the experiment for the local latitude (φ) of 42.5° in Odeillo. Table 2 gives the calculated solar angles – ω , δ , α , h – for the initial and final time of the experiment with no solar tracking, as well as the corresponding variation of the azimuth ($\Delta\alpha$) and altitude (Δh) angles.

Table 2. Calculated solar angles for the evaluation of the solar laser tracking error compensation capacity.

Solar angles	Initial time with no sun tracking, t_i	Final time with no sun tracking, t_f
Hour, ω	$-9.50^{\circ a}$	-8.34°
Declination, δ	19.16°	
Azimuth, α	-21.93°	-19.38°
Altitude, h	65.33°	65.63°
$\Delta\alpha$	2.54°	
Δh	0.30°	

^aThe experiment began 38 minutes before the local solar noon, so negative hour angles were calculated.

From the calculated values in Table 2, we can conclude that close to the local solar noon the azimuth angle contributes to the widest solar tracking error range. Consequently, the apparent focal spot displacement is higher in the azimuthal direction. Nevertheless, the wide pump cavity aperture of 68 mm along the optical axes of the laser rods, oriented in azimuthal direction,

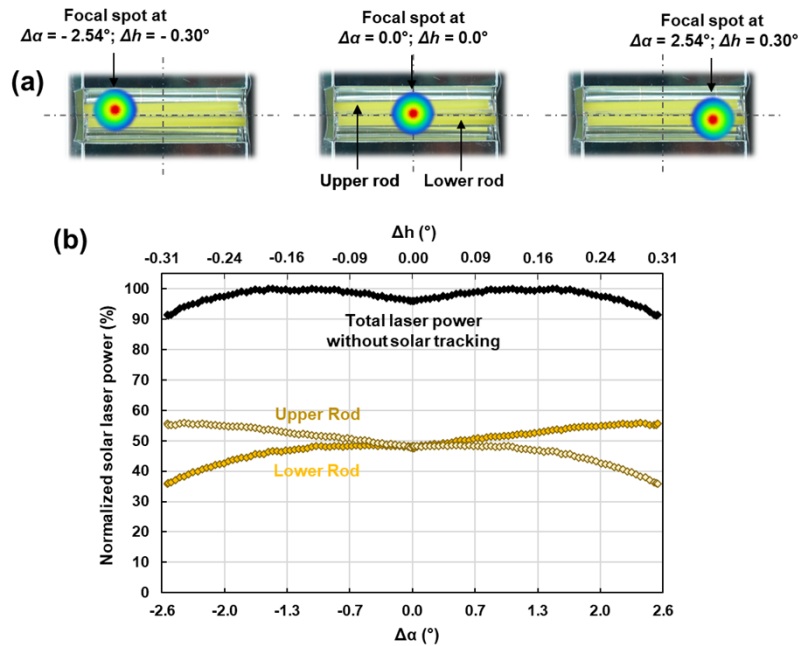


Fig. 7. (a) Schematic of the focal spot displacement on the entrance of the dual-rod pumping cavity at the maximum azimuth ($\Delta\alpha$) and altitude (Δh) angles with no solar tracking, as well as at optimal alignment ($\Delta\alpha = 0^\circ$; $\Delta h = 0^\circ$). (b) Normalized total solar laser output power, and the corresponding normalized laser power from each rod, as a function of both $\Delta\alpha$ and Δh angles.

enabled the parabolic mirror focal spot to remain inside it until the end of the experiment with no solar tracking, as represented in Fig. 7(a), corresponding to a maximum variation of the azimuth tracking error $\Delta\alpha$ of $\pm 2.54^\circ$.

As for the altitude angle, it only changed slightly with no solar tracking (Δh of $\pm 0.3^\circ$). This variation was sufficient to the displacement of the focal spot from the upper rod to the lower rod, leading to a decrease in the laser output power of the upper rod. However, this decrease was compensated by the increase in laser output power of the lower rod, resulting in less than 10% total solar laser power variation with no solar tracking, as observed in Fig. 7(b).

Figure 8 compares the maximum solar tracking error widths (TEW) in the azimuthal direction of the present dual-rod Ce:Nd:YAG solar laser with the previous measured from the dual-rod Nd:YAG solar laser [41]. While the total laser power from the previous scheme decreases by 10% at a tracking error width (TEW_{10%}) of 1.2° in the azimuthal direction, the total solar laser power from the dual-rod Ce:Nd:YAG solar laser scheme remains above 90% of the maximum power at a TEW of 5.1° , representing an enhancement of 4.25 times.

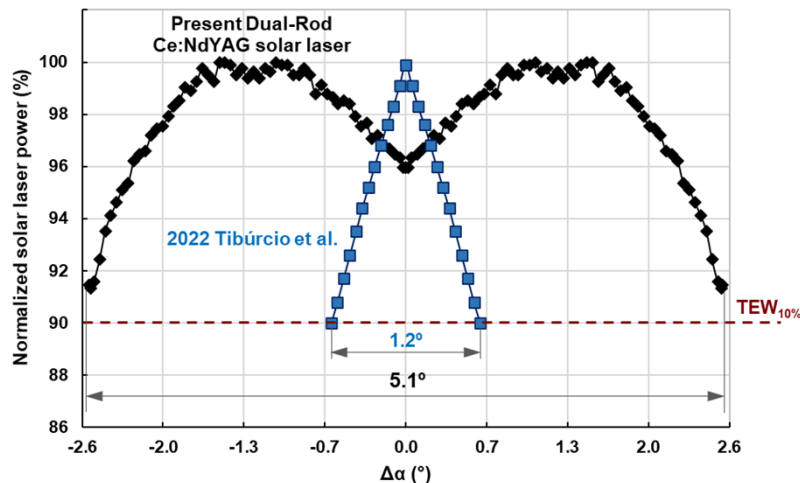


Fig. 8. Normalized total solar laser power from the present dual-rod Ce:Nd:YAG solar laser with no solar tracking and its comparison to the experimental results from the first solar laser with tracking error compensation measurements [41].

4. Conclusion

The potential of a dual-rod side-pumped Ce:Nd:YAG solar laser for both solar laser power scaling and higher tracking error compensation capacity was experimentally evaluated by the medium size solar facility of PROMES-CNRS. The alternative solar laser head with a dry pumping cavity combined the solar radiation coupling and redistribution capacity of the wide hollow pipe with the focusing capacity of both the biconical shaped reflectors and the fused silica flow tube, allowing efficient spreading of the highly concentrated solar radiation along the 3 mm diameter, 80 mm length Ce(0.1 at.):Nd(1.1 at.):YAG rods. This ensured not only the reduction of the thermal induced effects in Ce:Nd:YAG laser rods but also the substantial improvement in solar laser power. 58 W cw total solar laser power was detected with the maximum collection diameter of the parabolic mirror without damaging the laser rods. This was, to the best of our knowledge, the highest solar laser power reported from Ce:Nd:YAG media, being 1.45 times more than the previous record [30]. The threshold solar power was also reduced by 1.47 times in relation to previous scheme [30]. Moreover, collection, slope, and solar-to-laser conversion efficiencies of $25.3 \text{ W}\cdot\text{m}^{-2}$, 3.75% and 2.62% were respectively attained at maximum effective collection area

of 2.3 m², resulting in improvements of 1.57, 1.54 and 1.7 times over the previous values from the high-power single-rod Ce:Nd:YAG solar laser [29]. The obtained collection efficiency was also 1.07 times more than the previous record with side-pumped configuration [25]. Beyond the demonstrated potential to scale to high powers, the dual-rod solar laser head also proved its potential for high tracking error compensation. Thanks to the adoption of the side-pumping configuration with a wide pumping cavity, continuous solar laser operation with no solar tracking assistance was possible for 280 s. At the end of the experiment, the total laser power was still above 90% of its maximum value, enabling high tracking error compensation width of 5.1°, being more than four times wider than the previous record [41]. These breakthroughs with Ce:Nd:YAG gain media proved that, with an appropriate pumping configuration, it is possible to develop simpler and less expensive solar laser systems of high efficiency and stability, which may help to extend the applicability of this renewable technology either on earth or in space.

Funding. Fundação para a Ciência e a Tecnologia (EXPL/FIS-OTI/0332/2021, UIDB/00068/2020); Solar Facilities for European Research Area – Third Phase (SFERA III), (No. 823802).

Acknowledgments. Financial support of the strategic project UIDB/00068/2020 and the exploratory project EXPL/FIS-OTI/0332/2021 by FCT – MCTES is acknowledged. Financial support by the SFERA III, Grant Agreement No. 823802 is gratefully acknowledged. The FCT-MCTES grants CEECIND/03081/2017, SFRH/BD/145322/2019, 2021.06172.BD, and SFRH/BPD/125116/2016 of J. Almeida, M. Catela, H. Costa, and C. R. Vistas, respectively, are all acknowledged.

Disclosures. The authors declare no conflicts of interest.

Data availability. Data underlying the results presented in this paper are not publicly available at this time but may be obtained from the authors upon reasonable request.

References

1. C. Johnson, *Solar pumping converts broadband sunlight into efficient laser light*, Laser Focus World (Oct. 4, 2022).
2. C. Zhao, H. Zhang, Z. Guan, *et al.*, “Solar pumped Lasers for free space laser communication,” in *7th International Conference on Photonics, Optics and Laser Technology (PHOTOPTICS)*, (2019), pp. 268–275.
3. W. R. Weaver and J. H. Lee, “A solar pumped gas laser for the direct conversion of solar energy,” *J. Energy* **7**(6), 498–501 (1983).
4. R. J. Deyoung, G. D. Walberg, E. J. Conway, *et al.*, “A NASA high-power space-based laser research and applications program,” *NASA SP-464* (National Aeronautics and Space Administration, Washington DC, 1983).
5. L. David, *Space Junk Removal Is Not Going Smoothly*, Scientific American (Apr. 20, 2021).
6. M. Vasile and C. A. Maddock, “Design of a formation of solar pumped lasers for asteroid deflection,” *Adv. Space Res.* **50**(7), 891–905 (2012).
7. O. Graydon, “A sunny solution,” *Nat. Photonics* **1**(9), 495–496 (2007).
8. T. Okada, T. Saiki, S. Taniguchi, *et al.*, “Hydrogen Production Using Reduced-Iron Nanoparticles by Laser Ablation in Liquids,” *ISRN Renew. Energ.* **2013**, 1 (2013).
9. T. Motohiro, Y. Takeda, H. Ito, *et al.*, “Concept of the solar-pumped laser-photovoltaics combined system and its application to laser beam power feeding to electric vehicles,” *Jpn. J. Appl. Phys.* **56**(8S2), 08MA07 (2017).
10. Z. J. Kiss, H. R. Lewis, and R. C. Duncan, “Sun pumped continuous optical maser,” *Appl. Phys. Lett.* **2**(5), 93–94 (1963).
11. C. G. Young, “Sun-pumped cw one-watt laser,” *Appl. Opt.* **5**(6), 993–997 (1966).
12. H. Arashi, Y. Oka, N. Sasahara, *et al.*, “A solar-pumped cw 18 W Nd:YAG laser,” *Jpn. J. Appl. Phys.* **23**(8R), 1051–1053 (1984).
13. M. Weksler and J. Shwartz, “Solar-pumped solid-state lasers,” *IEEE J. Quant. Electron.* **24**(6), 1222–1228 (1988).
14. M. Lando, J. Kagan, B. Linyekin, *et al.*, “A solar-pumped Nd:YAG laser in the high collection efficiency regime,” *Opt. Commun.* **222**(1-6), 371–381 (2003).
15. D. Liang and J. Almeida, “Highly efficient solar-pumped Nd:YAG laser,” *Opt. Express* **19**(27), 26399–26405 (2011).
16. T. H. Dinh, T. Ohkubo, T. Yabe, *et al.*, “120 watt continuous wave solar-pumped laser with a liquid light-guide lens and an Nd:YAG rod,” *Opt. Lett.* **37**(13), 2670–2672 (2012).
17. D. Liang, J. Almeida, C. R. Vistas, *et al.*, “Solar-pumped Nd:YAG laser with 31.5 W/m² multimode and 7.9 W/m² TEM₀₀-mode collection efficiencies,” *Sol. Energy Mater. Sol. Cells* **159**, 435–439 (2017).
18. Z. Guan, C. Zhao, J. Li, *et al.*, “32.1 W/m² continuous wave solar-pumped laser with a bonding Nd:YAG/YAG rod and a Fresnel lens,” *Opt. Laser Technol.* **107**, 158–161 (2018).
19. D. Liang, J. Almeida, D. Garcia, *et al.*, “Simultaneous solar laser emissions from three Nd:YAG rods within a single pump cavity,” *Sol. Energy* **199**, 192–197 (2020).
20. V. Lupei, A. Lupei, C. Gheorghie, *et al.*, “Emission sensitization processes involving Nd³⁺ in YAG,” *J. Lumin.* **170**(2), 594–601 (2016).

21. B. Zhao, C. Zhao, J. He, *et al.*, “The study of active medium for solar-pumped solid-state lasers,” *Act. Opt. Sin.* **27**(10), 1797–1801 (2007).
22. T. Yabe, T. Ohkubo, S. Uchida, *et al.*, “High-efficiency and economical solar-energy-pumped laser with Fresnel lens and chromium codoped laser medium,” *Appl. Phys. Lett.* **90**(26), 261120 (2007).
23. D. Liang, C. R. Vistas, B. D. Tibúrcio, *et al.*, “Solar-pumped Cr:Nd:YAG ceramic laser with 6.7% slope efficiency,” *Sol. Energy Mater. Sol. Cells* **185**, 75–79 (2018).
24. C. R. Vistas, D. Liang, D. Garcia, *et al.*, “Ce:Nd:YAG continuous-wave solar-pumped laser,” *Optik* **207**, 163795 (2020).
25. C. R. Vistas, D. Liang, J. Almeida, *et al.*, “Ce:Nd:YAG side-pumped solar laser,” *J. Photon. Energy* **11**(01), 018001 (2021).
26. D. Garcia, D. Liang, C. R. Vistas, *et al.*, “Ce:Nd:YAG Solar Laser with 4.5% Solar-to-Laser Conversion Efficiency,” *Energies* **15**(14), 5292 (2022).
27. Z. Cai, C. Zhao, Z. Zhao, *et al.*, “Efficient 38.8 W/m² solar pumped laser with a Ce:Nd:YAG crystal and a Fresnel lens,” *Opt. Express* **31**(2), 1340 (2023).
28. D. Liang, C. R. Vistas, D. Garcia, *et al.*, “Most efficient simultaneous solar laser emissions from three Ce:Nd:YAG rods within a single pump cavity,” *Sol. Energy Mater. Sol. Cells* **246**, 111921 (2022).
29. C. R. Vistas, D. Liang, D. Garcia, *et al.*, “Uniform and Non-Uniform Pumping Effect on Ce:Nd:YAG Side-Pumped Solar Laser Output Performance,” *Energies* **15**(10), 3577 (2022).
30. J. Almeida, D. Liang, D. Garcia, *et al.*, “40 W Continuous Wave Ce:Nd:YAG Solar Laser through a Fused Silica Light Guide,” *Energies* **15**(11), 3998 (2022).
31. V. Lupei, A. Lupei, C. Gheorghe, *et al.*, “Spectroscopic and de-excitation properties of (Cr,Nd):YAG transparent ceramics,” *Opt. Mater. Express* **6**(2), 552–557 (2016).
32. S. Payziyev, A. Sherniyozov, S. Bakhrarov, *et al.*, “Luminescence sensitization properties of Ce: Nd: YAG materials for solar pumped lasers,” *Opt. Commun.* **499**, 127283 (2021).
33. M. Yamaga, Y. Oda, H. Uno, *et al.*, “Energy transfer from Ce to Nd in Y3Al5O12 ceramics,” *Phys. Status Solidi C* **9**(12), 2300–2303 (2012).
34. Y. Tai, G. Zheng, H. Wang, *et al.*, “Near-infrared quantum cutting of Ce³⁺–Nd³⁺ + co-doped Y3Al5O12 crystal for crystalline silicon solar cells,” *J. Photochem. Photobiol. A* **303–304**, 80–85 (2015).
35. M. Angulo-Calderón, I. Salgado-Tránsito, I. Trejo-Zúñiga, *et al.*, “Development and accuracy assessment of a high-precision dual-axis pre-commercial solar tracker for concentrating photovoltaic modules,” *Appl. Sci.* **12**(5), 2625 (2022).
36. H. Costa, D. Liang, J. Almeida, *et al.*, “Seven-Rod Pumping Concept for Highly Stable Solar Laser Emission,” *Energies* **15**(23), 9140 (2022).
37. M. Catela, D. Liang, C. R. Vistas, *et al.*, “Stable emission of solar laser power under non-continuous solar tracking conditions,” *Appl. Opt.* **62**(10), 2697–2706 (2023).
38. C. R. Vistas, D. Liang, M. Catela, *et al.*, “Fresnel Lens Solar Pumping for Uniform and Stable Emission of Six Sustainable Laser Beams under Non-Continuous Solar Tracking,” *Sustainability* **15**(10), 8218 (2023).
39. B. D. Tibúrcio, D. Liang, J. Almeida, *et al.*, “Dual-rod pumping approach for tracking error compensation in solar-pumped lasers,” *J. Photon. Energy* **9**(02), 1 (2019).
40. B. D. Tibúrcio, D. Liang, J. Almeida, *et al.*, “Highly efficient side-pumped solar laser with enhanced tracking-error compensation capacity,” *Opt. Commun.* **460**, 125156 (2020).
41. B. D. Tibúrcio, D. Liang, J. Almeida, *et al.*, “Tracking error compensation capacity measurement of a dual-rod side-pumping solar laser,” *Renew. Energy* **195**, 1253–1261 (2022).
42. D. Liang, J. Almeida, C. R. Vistas, *et al.*, *Solar-Pumped Lasers* (Springer Cham, 2023), Chap. 8.
43. J. Almeida, D. Liang, E. Guillot, *et al.*, “A 40W cw Nd:YAG solar laser pumped through a heliostat: a parabolic mirror system,” *Laser Phys.* **23**(6), 065801 (2013).
44. J. Almeida, D. Liang, C. R. Vistas, *et al.*, “Highly efficient end-side-pumped Nd:YAG solar laser by a heliostat–parabolic mirror system,” *Appl. Opt.* **54**(8), 1970–1977 (2015).
45. Z. Guan, C. Zhao, H. Zhang, *et al.*, “5.04% system slope efficiency solar-pumped Nd:YAG laser by a heliostat–parabolic mirror system,” *J. Photon. Energy* **8**(02), 1–8 (2018).
46. H. Mousazadeh, A. Keyhani, A. Javadi, *et al.*, “A review of principle and sun-tracking methods for maximizing solar systems output,” *Renew. Sust. Energy. Rev.* **13**(8), 1800–1818 (2009).
47. S. A. Kalogirou, *Solar Energy Engineering: Processes and Systems*, 2nd ed. (Elsevier, 2014).
48. V. Grigoriev, K. Milidonis, and M. Blanco, “Sun tracking by heliostats with arbitrary orientation of primary and secondary axes,” *Sol. Energy* **207**, 1384–1389 (2020).